Magnetic Resonance Elastography by Direct Visualization of Propagating Acoustic Strain Waves

Author(s): R. Muthupillai, D. J. Lomas, P. J. Rossman, J. F. Greenleaf, A. Manduca and R. L. Ehman

Source: *Science*, New Series, Vol. 269, No. 5232 (Sep. 29, 1995), pp. 1854-1857
Published by: American Association for the Advancement of Science
Stable URL: https://www.jstor.org/stable/2889267
Accessed: 28-03-2019 04:13 UTC

the HCHs) are readily distilled to colder, higher latitudes but that less volatile compounds (such as endosulfan and DDT) are not. Several factors appear to control the global distribution of these less volatile compounds: (i) chemical persistence in industrialized countries (such as the United States) where large amounts of these compounds were used in the past, (ii) present use in developing countries (such as India) where there is a market for inexpensive organochlorine compounds, and (iii) lack of use in countries (such as Ghana) that cannot afford to import and manufacture these compounds.

REFERENCES AND NOTES

1. F. Wania and D. Mackay, *Ambio* **22**, 10 (1993).
2. D. C. G. Muir *et al., Sci. Total Environ.* **160–161**, 447 (1995).
3. S. M. Chernyak *et al., ibid.*, p. 75.
4. D. Calamari *et al., Environ. Sci. Technol.* **25**, 1489 (1991).
5. H. Iwata *et al., ibid.* **27**, 1080 (1993).
6. D. Mackay and F. Wania, *Sci. Total Environ.* **160–161**, 25 (1995); F. Wania and D. Mackay, *ibid.*, p. 211.
7. B. Hileman, *Chem. Eng. News* **72**(5), 19 (31 January 1994); W. R. Kelce *et al., Nature* **375**, 581 (1995).
8. D. A. Hinckley, T. F. Bidleman, W. T. Foreman, J. R. Tuschall, *J. Chem. Eng. Data* **35**, 232 (1990).
9. Request for Proposal 223-95-2285 (Food and Drug Administration, Washington, DC, 1995); *Public Health Impact of Pesticides Used in Agriculture* (World Health Organization, Geneva, 1990), pp. 24–32.
10. E. C. Voldner and Y. F. Li, *Sci. Total Environ.* **160–161**, 201 (1995).
11. Remote or rural sites were generally chosen for sampling, and permission was obtained from land owners, park rangers, or other officials. Samples were collected as described in (*14*). A 5 cm by 20 cm area of outer bark was chiseled off the tree, wrapped in aluminum foil, and stored in a plastic bag. Two to three sites were usually sampled at the same time, and three to six samples were collected from different species of trees at each site. A permit for importing tree bark samples into the United States was obtained from the U.S. Department of Agriculture, Animal and Plant Health Inspections Services. Samples were shipped by various worldwide carriers and were stored at −18°C until extraction.
12. M. H. Hermanson and R. A. Hites, *Environ. Sci. Technol.* **24**, 666 (1990).
13. S. L. Simonich and R. A. Hites, *Nature* **370**, 49 (1994).
14. ———, *Environ. Sci. Technol.* **28**, 939 (1994).
15. Unground tree bark (wet weight, 30 to 50 g) was spiked with an appropriate amount of six isotopically labeled internal standards (d_6-γ-HCH, $^{37}Cl_6$-heptachlor epoxide, d_4-endosulfan I, $^{37}Cl_6$-*trans*-nonachlor, d_8-*p,p'*-DDE, and d_8-*p,p'*-DDT) and Soxhlet-extracted in 50% hexane in acetone for 24 hours. This procedure extracted the organochlorine compounds from the bark. All extracts were solvent-exchanged to hexane and back-extracted 2 to 10 times with high-performance liquid chromatography-grade water until the water fraction was not turbid. This procedure removed polar interferents and improved the subsequent silica gel separation. Extracts were then reduced to 1 ml and purified with a silica gel column (length 25 cm, deactivated with 1% water by weight). The compounds were eluted from the column with hexane (50 ml), 50% hexane in CH_2Cl_2 (75 ml), and CH_2Cl_2 (75 ml). HCB eluted in the hexane fraction, endosulfan II and endosulfan cyclic sulfate eluted in the CH_2Cl_2 fraction, and most of the other compounds eluted in the 50% hexane in CH_2Cl_2 fraction. All fractions were combined for analysis. Recoveries of known amounts of organochlorine compounds were 76 to 84% for the entire procedure. Reagent blanks were done with every other set of extractions, and the blank experiments were free of contamination.
16. The gas chromatograph (GC) was equipped with a 30 m by 250 μm inside diameter (film thickness 0.25 μm) DB-5 fused silica capillary column (J&W Scientific, Folsom, CA). The ion source was maintained at a temperature of 125°C and a CH_4 pressure of 0.43 torr (direct source reading). After concentration to 200 μl under a gentle stream of N_2, 1 μl of the sample was injected splitless for 0.9 min. The GC temperature program conditions were 40°C held for 1 min, ramped at 30°C/min to 130°C, then at 3°C/min to 241°C, and finally at 30°C/min to 285°C and held for 10 min. The GC was set for a constant head pressure of 15 psi. The combination of these GC conditions and the selected ion monitoring program allowed us to analyze all 22 compounds in one injection. The detection limit ranged from 2 to 500 pg, depending on the electron-capture cross section of the analyte.
17. D. J. Anderson and R. A. Hites, *Atmos. Environ.* **23**, 2063 (1989); H. R. Buser and M. D. Muller, *Environ. Sci. Technol.* **27**, 1211 (1993).
18. *Insect Control Guide* (Meister, Willoughby, OH, 1995).
19. HCB, α- and γ-HCH, and PCA have subcooled liquid vapor pressures on the order of 0.1 to 0.01 Pa (at 25°C); see (*8*).
20. P. Tremolada *et al.*, *Chemosphere* **27**, 2235 (1993); D. Calamari *et al.*, *Environ. Sci. Technol.* **28**, 429 (1994).
21. S. L. Simonich, thesis, Indiana University (1995).

22. We thank more than 70 scientists, friends, and colleagues who helped in the collection of samples.

24 April 1995; accepted 13 July 1995

Magnetic Resonance Elastography by Direct Visualization of Propagating Acoustic Strain Waves

R. Muthupillai, D. J. Lomas, P. J. Rossman, J. F. Greenleaf, A. Manduca, R. L. Ehman*

A nuclear magnetic resonance imaging (MRI) method is presented for quantitatively mapping the physical response of a material to harmonic mechanical excitation. The resulting images allow calculation of regional mechanical properties. Measurements of shear modulus obtained with the MRI technique in gel materials correlate with independent measurements of static shear modulus. The results indicate that displacement patterns corresponding to cyclic displacements smaller than 200 nanometers can be measured. The findings suggest the feasibility of a medical imaging technique for delineating elasticity and other mechanical properties of tissue.

The spatial and temporal pattern of strain created within solid objects subjected to dynamic mechanical stress is of great interest in many disciplines of science and engineering. For instance, the dynamic strain distribution associated with propagation of shear and compression waves is of substantial importance in materials science and in ultrasonics, where such information may be used to predict dynamic behavior and demonstrate structural integrity and composition. However, there have been few noninvasive methods for measuring the three-dimensional strain effects (or strain dyadic) created by mechanical waves within materials (*1*). We describe a method to spatially map and quantitate displacement patterns corresponding to harmonic mechanical waves with amplitudes of 1 μm or less in tissue and other materials with a nuclear magnetic resonance (NMR) technique. Strain and other mechanical characteristics related to wave propagation can be computed from these displacement patterns. Such images could be used to noninvasively deduce important mechanical properties of the internal structure of a wide range of solid materials.

In the presence of a magnetic-field gradient, the motion of nuclear spins causes a phase shift ϕ in an NMR signal (*2*) given by

$$\phi = \gamma \int_0^{\tau} \mathbf{G}_r(t) \cdot \mathbf{r}(t) dt \qquad (1)$$

where γ is the gyromagnetic ratio characteristic of the nuclei, τ is the time duration of the gradients after excitation, $\mathbf{G}_r(t)$ is a temporal function of the magnetic gradient superimposed on the static magnetic field $\mathbf{B}_0$, and $\mathbf{r}(t)$ describes the position of the nuclear spins as a function of time.

If $\mathbf{r}(t)$ represents simple linear motion, then

$$\mathbf{r}(t) = \mathbf{r}_0 + \mathbf{v}_0 t \qquad (2)$$

where $\mathbf{r}_0$ and $\mathbf{v}_0$ are, respectively, the position and velocity at time $t = 0$. If the acceleration and higher order terms are negligible, then given an appropriate gradi-

R. Muthupillai, P. J. Rossman, J. F. Greenleaf, A. Manduca, R. L. Ehman, Mayo Clinic and Foundation, Rochester, MN 55905, USA.
D. J. Lomas, Department of Radiology, Addenbrooke's Hospital, Cambridge, UK.
*To whom correspondence should be addressed.

ent function $\mathbf{G}_r(t)$, Eq. 1 establishes a simple relation between the phase shift of the NMR signal and the first gradient moment (*3*, *4*), which is used to estimate blood flow velocity in clinical MRI (*5*–*7*).

Complex motion may be described by

$$\mathbf{r}(t) = \mathbf{r}_0 + \vec{\xi}(\mathbf{r},t) \qquad (3)$$

where $\mathbf{r}_0$ is the mean position of the nuclear spin and $\vec{\xi}(\mathbf{r}, t)$ is the displacement of the spin about its mean position. In Eq. 1, $\mathbf{G}_r(t)$ may be viewed as a basis function for estimating the harmonic components of nuclear spin position $\mathbf{r}(t)$, and a set of such functions, mutually orthogonal over the integral duration, could be defined for estimation of an arbitrary $\mathbf{r}(t)$.

Consider the specific case in which the nuclear spins undergo simple harmonic motion about their mean position $\mathbf{r}$

$$\vec{\xi}(\mathbf{r}, \theta) = \vec{\xi}_0\cos(\mathbf{k}\cdot\mathbf{r} - \omega t + \theta) \qquad (4)$$

where $\mathbf{k}$ is the wave vector, θ is an initial phase offset, ω is the angular frequency of the mechanical excitation, and $\vec{\xi}_0$ is the displacement amplitude. Under these circumstances, it is useful to consider a basis function gradient $\mathbf{G}_r(t)$ that is switched in polarity at the same frequency as the nuclear spin motion (*8*). If the time duration τ is chosen so that $\int_0^\tau \mathbf{G}_r(t)dt = 0$, then the observed phase shift in the NMR signal is given by

$$\phi(\mathbf{r},\theta) = \gamma \int_0^{\tau = NT<TE} \mathbf{G}_r(t)\cdot\vec{\xi}_0\cos(\mathbf{k}\cdot\mathbf{r} - \omega t + \theta)dt \qquad (5)$$

$$= \frac{2\gamma NT(\mathbf{G}\cdot\vec{\xi}_0)}{\pi}\sin(\mathbf{k}\cdot\mathbf{r} + \theta)$$

where N is the number of gradient cycles, T is the period of the mechanical excitation, TE is the time at which the NMR signal is received, and $\omega = 2\pi/T$. Equation 5 indicates that the observed phase shift in the NMR signal obtained under these conditions is proportional to the scalar product of the displacement amplitude vector and the gradient vector and to N. This latter dependence increases sensitivity to small-amplitude oscillatory motion by accumulating phase shifts over multiple cycles of the mechanical excitation and synchronous gradient wave form. By considering the gradient function as a basis function, it is possible to "filter" out harmonic coefficients of arbitrary motion in view of the scalar product.

To test the hypothesis that the proposed method can be used to quantitatively image the characteristics of propagating mechanical waves, we performed experiments with a whole-body NMR tomography system (*9*) (Fig. 1). The pulse sequence controlling the MRI system used conventional phase- and frequency-encoding gradients to allow image reconstruction with a two-dimensional Fourier transformation algorithm (*10*). The sequence incorporated harmonic motion–sensitizing gradient wave forms and synchronous trigger pulses, which were fed to a wave-form generator driving an electromechanical actuator. A balanced acquisition scheme was used to suppress systematic phase errors while doubling the phase sensitivity of the system (*11*–*13*). Typical acquisition parameters were pulse repetition times (TR) of 40 to 300 ms, echo delay times (TE) of 20 to 60 ms, section thicknesses of 10 mm, 128 to 256 phase-encoding views, and image acquisition times of 10 to 120 s.

Figure 2 shows results obtained from a uniform agarose gel phantom, with shear waves applied at two discrete points on the surface. The pixel values of the phase image (Fig. 2B) vary sinusoidally as predicted by Eq. 5, with wavelength λ (where $\lambda = 2\pi/|\mathbf{k}|$) in the direction of wave propagation, depending on the temporal phase relation between the strain wave and the harmonic motion–sensitizing gradient at each position in the image. By solving Eq. 5 for the

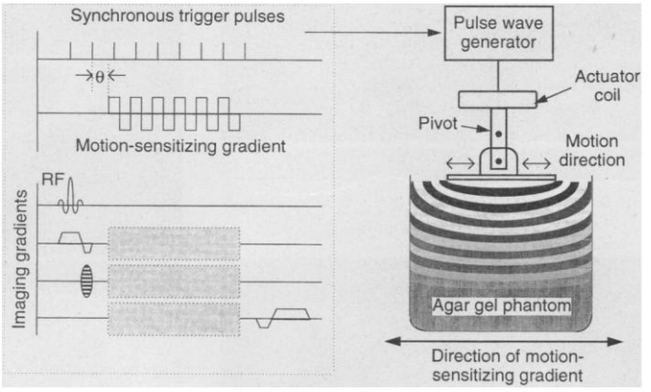

Fig. 1. Experimental system for observing acoustic strain waves with MRI. A gradient-echo imaging pulse sequence was modified to incorporate a gradient wave form for sensitizing the sequence to harmonic motion and to generate synchronous pulses for triggering the motion of an electromechanical actuator. The actuator consists of an electrical coil attached to a pivot bar and is driven by a wave generator at 50 to 1000 Hz. The alternating flux of the coil interacts with the main magnetic field of the imager, yielding a cyclic force, which is coupled by a contact plate to the surface of the object to be studied. The period and the number of motion-sensitizing gradient pulses are adjustable, as is the phase relation (θ) between the cyclic gradient wave form and the trigger pulses. An adjustable number of trigger pulses can be applied before the initial radio frequency (RF) excitation to establish a mechanical steady state. The motion-sensitizing gradients can be applied along any desired axis (indicated by shaded regions) in combination with the imaging gradients.

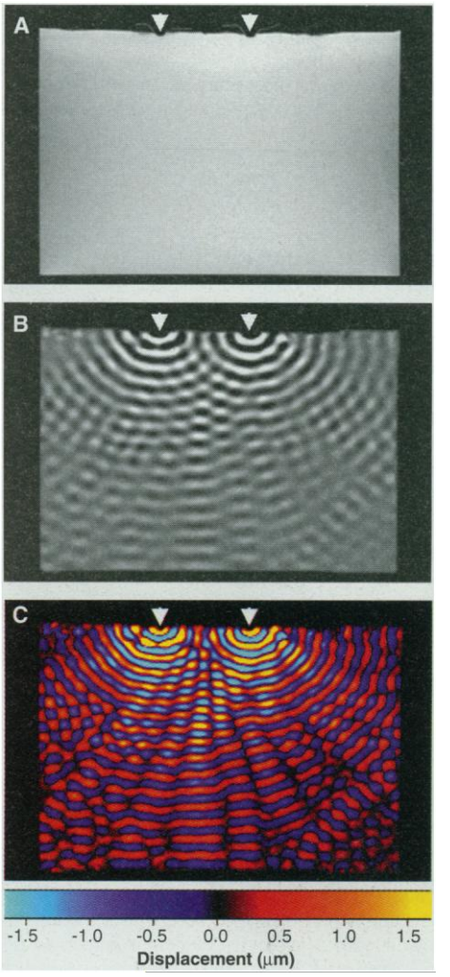

Fig. 2. Propagating shear waves. (**A**) Spin-echo MR image showing a uniform tissue-simulating gel object measuring 20 cm transversely. Acoustic shear wave excitation (500 Hz) was applied at two discrete points (arrowheads) separated by 54 mm, with the transverse motion of 2 μm directed perpendicular to the image plane. (**B**) The strain-wave imaging sequence illustrated in Fig. 1 was used with the harmonic motion–sensitizing gradient (20 cycles) directed perpendicular to the image plane. This phase image demonstrates a pattern of phase shifts corresponding to shear waves propagating from each source. Various wave properties such as wavelength and attenuation are depicted, as well as a classic dual-source interference pattern with regions where phase shifts add constructively and destructively. (**C**) Using Eq. 5, we converted the phase shifts (A) to displacement values encoded in a color scale to emphasize the quantitative nature of the method.

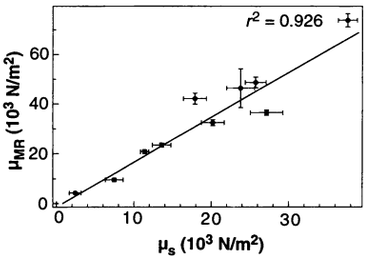

Fig. 3. Comparison of NMR and mechanical estimates of shear modulus. The static shear modulus μ_s was measured with a mechanical displacement–load compression technique (*17, 18, 22, 23*) in a series of 10 different agarose gel specimens (1.0 to 2.6 weight %) with varying stiffness. Before mechanical testing, NMR strain-wave imaging was performed on the same specimens, at a shear-wave frequency of 300 Hz. The wavelength (λ) of the shear waves in the uniform gel specimens was measured in the displacement images. The magnitude of the shear modulus (μ_{MR}) was computed from the relation $\mu = \nu^2\lambda^2\rho$, where ν is the frequency of excitation and ρ is the density of the medium (*24*). The two independent estimates of shear modulus are well correlated ($r^2 = 0.926$, $\mu_{MR} = 1.88\ \mu_s - 1.41$). The slope of the graph is not unity because the MR estimate of shear modulus incorporates both elastic and viscous components of the complex shear modulus (*24*). In addition, the NMR estimate is based on microscopic displacements, whereas the mechanical estimate is based on much larger strain values that lead to nonlinearities as a result of creep and other phenomena (*23*).

proportionality constant relating the displacement to NMR phase shift, we are able to depict the displacement at each point in the image quantitatively (Fig. 2C). An independent measure of displacement at the surface was obtained with an optical deflection method (*14*) over a range of 0 to 60 μm; all experiments were performed within this range. The displacements computed from the MR images were in good agreement with those obtained with the optical technique (correlation coefficient r^2 = 0.955).

Comparison between MRI-derived estimates of shear modulus (μ_{MR}) and independently obtained measurements of static shear modulus (μ_s) (Fig. 3) support the hypothesis that the technique can be used to quantitatively probe the mechanical characteristics of material. A nonuniform object containing two agarose gel cylinders with high and low stiffness embedded in intermediate-stiffness agar gel was studied. The resulting displacement image (Fig. 4A) reflects shear wave propagation in a medium of varying stiffness. The local wavelength of the shear waves was calculated at each location in the image (*15*). These data were then used to compute the local shear modulus, with a mean density of 1.0 g/cm^3, which is appropriate for tissue-equivalent gels and soft tissues (*16*). The resulting image (Fig. 4B) provides an estimate of the local shear modulus at each location in the section through the object.

To test the feasibility of using the technique to image the mechanical properties of tissues, we imaged a porcine kidney specimen using shear-wave excitation at 200 and 400 Hz (Fig. 5). The computed shear modulus image demonstrated a rim with high shear modulus in the peripheral cortex of the kidney, distinct from the medullary region and the surrounding gel. Experiments to assess the sensitivity of the strain-wave imaging method at low amplitudes of mechanical excitation demonstrated that shear waves with displacements of less than 100 nm could be readily observed.

Prior attempts to assess the mechanical properties of tissues have used Doppler ultrasound to assess tissue motion in response to low-frequency strain waves (*17, 18*). These methods are constrained by limited lateral resolution and low sensitivity. An ultrasound technique (*19*) and a phase-contrast MR technique (*20*) using nonharmonic static or repeated "single shot" mechanical excitation to assess mechanical properties have been described. These techniques in general require knowledge of boundary conditions or analytical solutions to compute the mechanical moduli, which may be difficult to obtain. The possibility of using a spectroscopic NMR technique to detect Larmor frequency modulations caused by longitudinal mechanical waves in the presence of a constant gradient has been suggested (*21*), but the sensitivity and feasibility of imaging with such a technique is yet to be determined. Also, at low frequencies the wavelength of longitudinal waves typically far exceeds the size of the objects being imaged. Potential advantages of the MR elastography (MRE) method described

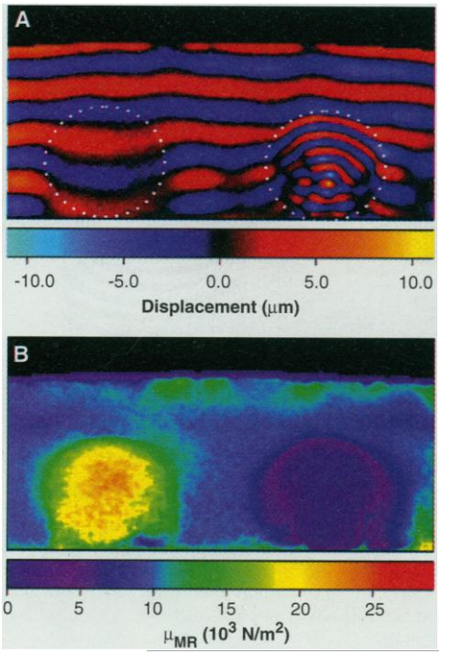

Fig. 4. Magnetic resonance elastography. A tissue-simulating gel object containing two embedded gel cylinders (dotted lines, 44-mm diameter) with differing stiffness was imaged. Shear-wave excitation at 250 Hz (perpendicular to the image plane) with a lateral-displacement amplitude of 5.0 μm was applied to a wide contact plate on the surface. (**A**) This NMR displacement image demonstrates planar shear waves propagating down from the surface. The cylinder on the left is stiffer than the surrounding gel, resulting in a wavelength larger than that in surrounding gel. Conversely, the wavelength in the softer gel cylinder on the right is shorter than that in surrounding gel. The image also demonstrates refraction phenomena, causing a focusing effect within the softer cylinder. (**B**) Quantitative map of shear modulus (μ_{MR}) computed from the local wavelength of the displacement image. The NMR-estimated shear modulus of the plug on the left, for instance, is ~22 kN/m^2, in good agreement with earlier measurements of large homogeneous samples of the same gel (23.8 kN/m^2).

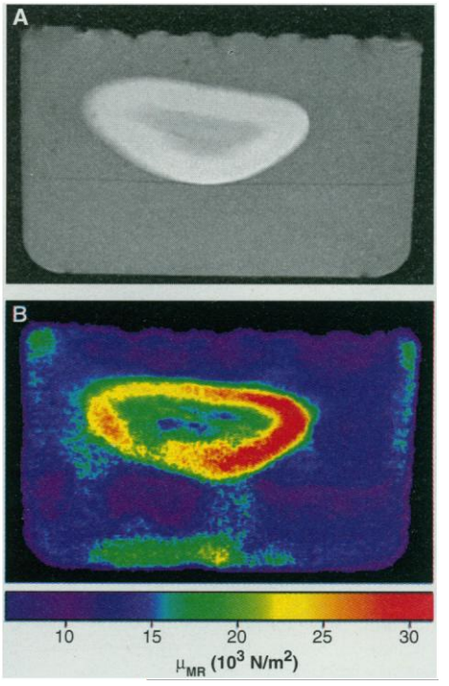

Fig. 5. Porcine kidney. (**A**) Conventional gradient echo image of a fresh kidney specimen embedded in gel demonstrates renal cortex surrounding renal medulla. (**B**) MR elastogram computed from wavelength data averaged from four images each at 200- and 400-Hz shear-wave excitation. The superficial layer of the cortex has a shear modulus of 21 to 30 kN/m^2, distinctly higher than that of the medulla.

here include direct quantitative imaging of cyclic displacements as small as 100 nm, a freely oriented field of view unencumbered by the "acoustic window" required for ultrasound-based techniques, and the ability to study strain-wave propagation in a dynamic fashion. The flexibility of NMR methodology allows the motion-sensitizing gradient to be placed along any axis, so that with multiple acquisitions it is, in principle, feasible to estimate all components of the strain dyadic.

Two general fields of application for this technique are anticipated. The first is the study and visualization of strain-wave propagation within objects or materials that can be imaged with MRI. In principle, the method can depict the spatial patterns of wave propagation characteristics such as divergence, scatter, attenuation, interference, diffraction, and dispersion. If at least one full cycle of mechanical excitation is applied within the TE interval of the NMR sequence, then the practical low frequency limit is ~10 Hz. The upper frequency limit is determined by the maximum slew rate of the gradient system of the imager and is in the range of 1 to 2 kHz if the motion-sensitizing gradient oscillates at the same frequency as the mechanical excitation. Our experiments have shown that we can image mechanical-excitation wave forms ranging from continuous waves to repeated short wave trains or even single cycles of mechanical excitation repeated each TR cycle.

A second general area of application is to apply mechanical strain wave excitation to interrogate the properties of materials within a heterogeneous object. Elastic moduli are of special interest in the context of medical applications. For centuries, physicians have used palpation of the body to detect the presence of tumors and other diseases. Unfortunately, many structures of the body are not accessible to the palpating hand. It is not unusual at the time of abdominal laparotomy for surgeons to discover tumors by direct palpation of abdominal organs that have gone undetected in prior imaging by computed tomography, ultrasound, or conventional MRI. In addition to potentially providing a noninvasive "palpation" technique that extends the reach and resolution of the diagnostic method, MRE offers the possibility of providing other measurable viscoelastic parameters such as attenuation and dispersion as criteria for further tissue characterization. We speculate that MRE may have a role in the detection of tumors of the breast, liver, kidney, and prostate.

REFERENCES AND NOTES

1. H. Kolsky, *Stress Waves in Solids* (Dover, New York, ed. 1, 1963), pp.131–168.
2. E. L. Hahn, *J. Geophys. Res.* **65**, 776 (1960).
3. The first gradient moment is defined as $\int_0^\tau \mathbf{G}_r(t)tdt$, where $\mathbf{G}_r(t) = G_x\hat{i} + G_y\hat{j} + G_z\hat{k}$.
4. P. R. Moran, *Magn. Reson. Imaging* **1**, 197 (1982).
5. P. van Dijk, *J. Comput. Assist. Tomogr.* **8**, 429 (1984).
6. D. J. Bryant *et al.*, *ibid.*, p. 588.
7. L. R. Pelc *et al.*, *Radiology* **185**, 809 (1992).
8. The applied switching polarity gradient is given by

$$\mathbf{G}_r(t) = \begin{cases} +|G| \text{ for } (n-1)T < \tau < (2n-1)T/2 \\ -|G| \text{ for } (2n-1)T/2 < \tau < nT \end{cases}$$

where $n = 1, 2, \ldots N$ and $\tau = NT$.
9. 1.5-T General Electric Medical Systems Signa; Milwaukee, WI.
10. A. Kumar, D. Welti, R. R. Ernst, *J. Magn. Reson.* **18**, 69 (1975).
11. The pulse sequence is performed twice for each phase-encoding view with motion-sensitizing gradients of opposite polarity. The two reconstructed data sets are subtracted to yield phase-difference images, analogous to methods used for phase-contrast MR angiography (*12, 13*).
12. C. L. Dumoulin and H. R. Hart, *Radiology* **161**, 717 (1986).
13. N. J. Pelc, M. A. Bernstein, A. Shimakawa, G. H. Glover, *J. Magn. Reson. Imaging* **1**, 405 (1991).
14. The displacement at the driving surface was measured by observing the deflection of a laser beam reflected from a mirror attached to the pivoting mechanical actuator.
15. H. Knutsson, C. J. Westin, G. Granland, *Proceedings of the IEEE International Conference on Image Processing-94* (IEEE Computer Society Press, Los Alamitos, CA, ed. 1, 1994), p. 36.
16. M. M. Burlew *et al.*, *Radiology* **134**, 517 (1980).
17. K. J. Parker, S. R. Huang, R. A. Musulin, R. M. Lerner, *Ultrasound Med. Biol.* **16**, 241 (1990).
18. S. R. Huang, thesis, University of Rochester, Rochester, NY (1990).
19. J. Ophir, I. Cespedes, H. Ponnekanti, Y. Yazdi, X. Li, *Ultrason. Imaging* **13**, 111 (1991).
20. D. B. Plewes, I. Betty, I. Soutar, *Proc. Soc. Magn. Reson.* **1**, 410 (1994).
21. C. J. Lewa and J. D. de Certaines, *J. Magn. Reson. Imaging* **5**, 241 (1995).
22. For purposes of testing, a Poisson ratio of 0.495 was assumed.
23. Y. C. Fung, *Biomechanics: Mechanical Properties of Living Tissues* (Springer-Verlag, New York, ed. 1, 1981), pp. 35–38.
24. E. L. Madsen, H. J. Sathoff, J. A. Zagzebski, *J. Acoust. Soc. Am.* **74**, 1346 (1983).

25. We gratefully acknowledge the contributions of S. J. Riederer, K. N. An, and J. J. Grabowski to this work. Partially supported by NIH grant CA51124.

24 April 1995; accepted 20 July 1995

Anisotropy and Spiral Organizing Centers in Patterned Excitable Media

Oliver Steinbock, Petteri Kettunen, Kenneth Showalter*

Chemical wave behavior in a patterned Belousov-Zhabotinsky system prepared by printing the catalyst of the reaction on membranes with an ink jet printer is described. Cellular inhomogeneities give rise to global anisotropy in wave propagation, with specific local patterns resulting in hexagonal, diamond, and pentagonal geometries. Spiral wave sources appear spontaneously and serve as organizing centers of the surrounding wave activity. The experimental methodology offers flexibility for studies of excitable media with made-to-order spatial inhomogeneities.

Propagating waves are observed in living organisms and biological tissues (*1*) as well as excitable chemical systems (*2*). The familiar rotating spiral waves and expanding target patterns of the Belousov-Zhabotinsky (BZ) reaction (*3*) are also observed in thin slices of heart tissue (*4*), in the cytoplasm of frog oocytes (*5*), and in animal retinas (*6*). Three-dimensional scroll waves, extensively studied in the BZ reaction (*7*), have now been characterized in migrating slugs of the slime mold *Dictyostelium discoideum* (*8*), and it is likely that these waves are precursors to ventricular fibrillation in mammals (*9*). The cellular nature of living systems, however, gives rise to inhomogeneities and anisotropy not present in homogeneous reaction systems, and these may play an important role in the behavior of biological media. A crucial example is found in the anisotropy of mammalian heart muscle (*10*). The cellular structure of cardiac tissue not only causes local variations in wave velocity (*4*) but also gives rise to propagation failure (*11*). In this report, we describe wave behavior in excitable media with well-defined cellular inhomogeneities obtained by printing catalyst patterns on a BZ-membrane system. Our experimental and numerical investigations show that local patterns determine the global wave geometry and give rise to spontaneous organizing centers.

Noszticzius and co-workers (*12*) have recently demonstrated that bathoferroin, a catalyst and indicator for the BZ reaction (*13*), is effectively immobilized on polysulphone membranes. Our experimental method is based on the precision loading of this catalyst onto the membranes with an ink jet printer (*14*). Patterns were generated as black and white images by a commercial graphics program, which were then printed with the catalyst solution on the polysulphone membranes. Following Noszticzius (*12*), the ready-to-use membranes were

Department of Chemistry, West Virginia University, Morgantown, WV 26506–6045, USA.

*To whom correspondence should be addressed.